Supporting Information

TADF Sensitizer Moiety Decorated MR Emitter Enhancing Spin-flip and Anti-ACQ

Xingtian Wang,[a] Jianxing Chen,[a] Songqian Ni,[a] Yu Hu,[a] Haorun Dai,[a] Zezhu Xiao,[a] Weiguo Zhu,[a] Pi-Tai Chou,[b]*and Xiugang Wu[a]*

[a] *School of Materials Science and Engineering, Jiangsu Engineering Laboratory of Light-Electricity-Heat Energy-Converting Materials and Applications, Jiangsu Collaborative Innovation Center of Photovoltaic Science and Engineering, Changzhou, 213164, China*

**To whom correspondence should be addressed. Email:*

(X. W.) xgwu16@cczu.edu.cn

(P.-T.Chou) chop@ntu.edu.tw

1. Experimental Section

General Information

^{1}H and ^{13}C NMR spectra were measured on a Bruker Avance III 400 and 500 MHz NMR spectrometer using $CDCl_3$ as the solvent and tetramethylsilane as an internal standard at room temperature. A suitable crystal was selected, and three-dimensional X-ray data were collected on a Bruker D8 Venture diffractometer. The diffraction experiments were carried out at 100 K during data collection. Thermogravimetric analysis (TG-DTA) was performed by Bruker TG-DTA 2400SA with a heating rate of 10 ℃ min^{-1} from 40 ℃ to 600 ℃ under a nitrogen atmosphere.

ITO substrates (0.5 cm × 1 cm) were cleaned with isopropyl alcohol, acetone, detergent, and deionized water in an ultrasonic bath, followed by a 15-minute UV-ozone treatment. The solution was subsequently spin-coated at 1000 rpm for 60 s inside the glove box on cleaned ITO substrates.

Reagents and materials

Materials were purchased from commercial suppliers and were used after appropriate purification, unless otherwise noted.

Device fabrication and characterization:

The OLED devices were fabricated using solution-processed method with device structure of ITO/PEDOT:PSS (35nm)/ EML (30nm)/ TmPyPB (45nm) /LiF (1nm) /Al (120nm), where ITO is indium tin oxide as anode, PEDOT: PSS is poly(3,4-ethylene-dioxythiophene) /poly(styrenesulfonate) (AI 4083) as hole injection layer, PhCzBCz is 9-(2-(9-phenyl-9H-carbazol-3-yl)phenyl)-9H-3,9′-bicarbazole as host material, TmPyPB is 3,3'-(5'-(3-(pyridin-3-yl)phenyl)-[1,1':3',1"-terphenyl]-3,3"-diyl)dipyridine as electron transporting layer, LiF is lithium fluoride as electron-injection layer and Al is aluminum as cathode, respectively. The substrates are pre-treated by oxygen plasma to increase the work function of the ITO film. Then, 30 nm-thick PEDOT: PSS was spin-coated onto the ITO substrates at 3000 rpm for 30 s and annealed at 150 °C for 15 min. And then the emissive layer was spin-coated and annealed at 60 °C for 30 min using a precursor containing different materials co-dissolved in chlorobenzene. The films of TmPyPB, LiF, and aluminum were prepared by thermal evaporation under a vacuum of 3×10^{-4} Pa. Each sample has an active area of 0.04 cm^2. All the devices were encapsulated before characterization to prevent degradation and emission quenching caused by oxygen and water. The EL spectra and J–V–L curves were obtained with a PHOTORESEARCH Spectra Scan PR735 photometer and a KEITHLEY 2400 Source Meter constant current source at room temperature. The EQE values were calculated by assuming a Lambertian distribution.

2. Synthesis of the materials

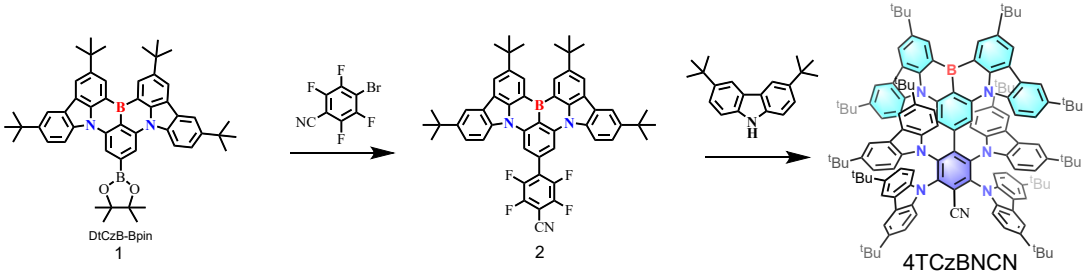

Fig. S1. Synthetic route of 4TCzBNCN.

Synthesis of (2): A mixture of 1 (1.0g, 1.3 mmol), 4-bromo-2,3,5,6-tetrafluorobenzonitrile (0.31g, 1.19mmol), K_2CO_3 (0.72 g, 4.2 mmol), and $Pd(PPh_3)_4$ (0.14g, 0.12 mmol) in toluene (30 mL): ethanol (6 mL) was stirred for 12 h at 100 ℃ under nitrogen. After cooling to room temperature, the reaction mixture was added to water and then extracted with CH_2Cl_2. The collected organic layer was washed with water and dried over anhydrous Na_2SO_4, then evaporated under reduced pressure. The crude product was further purified by column chromatography on silica gel (eluent: hexane/CH_2Cl_2 = 8:1, v/v). After removal of the solvents by evaporation, the resulting solid was dried under vacuum to give the desired product 2 as an orange solid (yield = 0.82 g, 76.8%). ^{1}H NMR (400 MHz, Chloroform-d) δ 9.14 (s, 2H), 8.50 (s, 2H), 8.39 (s, 2H), 8.28 (s, 3H), 7.67 (d, J = 9.0 Hz, 3H), 1.68 (s, 18H), 1.53 (s, 18H). ^{13}C NMR (100 MHz, Chloroform-*d*) δ 144.89, 144.17, 143.11, 140.50, 136.96, 128.82, 126.10, 123.69, 122.80, 120.16, 116.44, 112.66, 107.88, 34.19, 33.82, 31.11, 30.75.

Synthesis of 4TCzBNCN: The mixture of products **2** (1.0 g, 1.23 mmol), 9H-carbazole (1.72 g, 6.15 mmol) and NaH (0.3 g, 12.3 mmol) in dried N,N-dimethylformamide (60 mL) was stirred at 115 °C for 12 h. After cooling to room temperature, the reaction mixture was added to water and then extracted with CH_2Cl_2. The collected organic layer was washed with water and dried over anhydrous Na_2SO_4, then evaporated under reduced pressure. The crude product was further purified by column chromatography on silica gel (eluent: hexane/CH_2Cl_2= 8:1, v/v). After removal of the solvents by evaporation, the resulting solid was dried under vacuum to give 4TCzBNCN as an yellow solid (yield = 0.86 g, 38.3%). ^{1}H NMR (400 MHz, Chloroform-d) δ 7.84 (s, 4H), 7.56 (d, J = 10.0 Hz, 8H), 7.28 (d, J = 1.8 Hz, 2H), 6.94 (s, 10H), 6.76 (s, 8H), 6.04 (d, J = 8.7 Hz, 4H), 1.38 – 1.23 (m, 108H).^{13}C NMR (100 MHz, Chloroform-*d*) δ 144.38, 143.47, 143.03, 142.80, 140.97, 137.88, 137.70, 137.60, 136.70, 129.40, 126.59, 124.33, 123.91, 123.87, 123.28, 122.83, 122.12, 120.16, 116.92, 115.71, 113.65, 109.87, 109.49, 108.82, 35.01, 34.63, 34.57, 34.25, 32.06, 31.95, 31.87, 31.73.

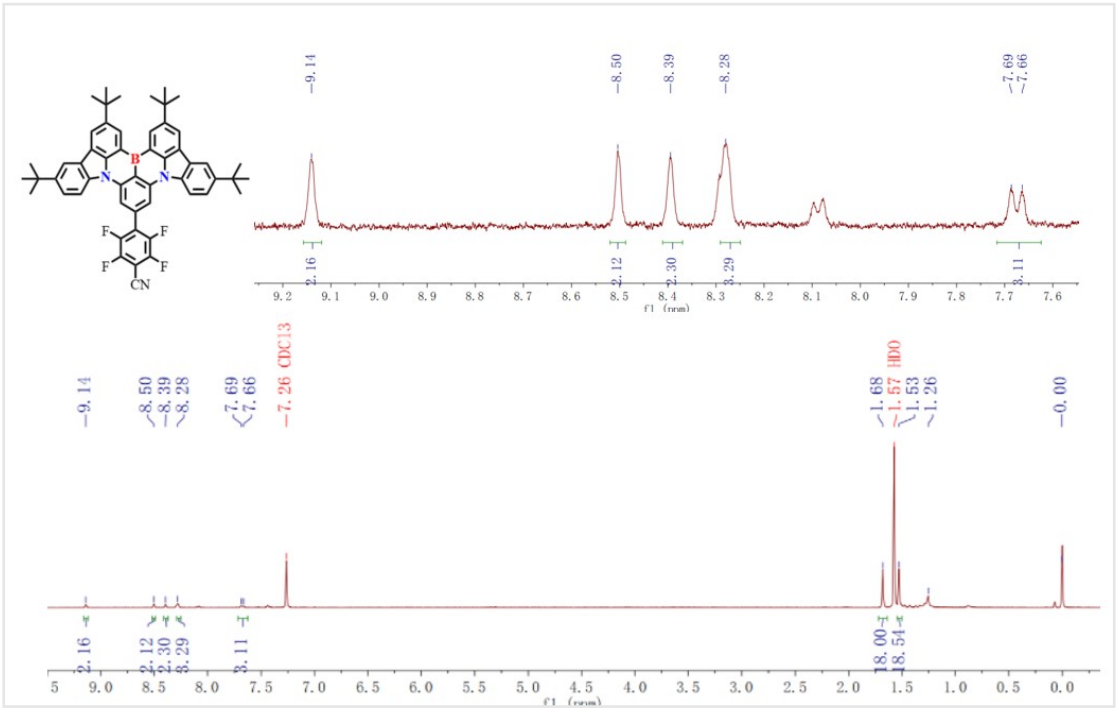

Fig. S2. ^{1}H-NMR spectrum of compound 2 in $CDCl_3$ at room temperature.

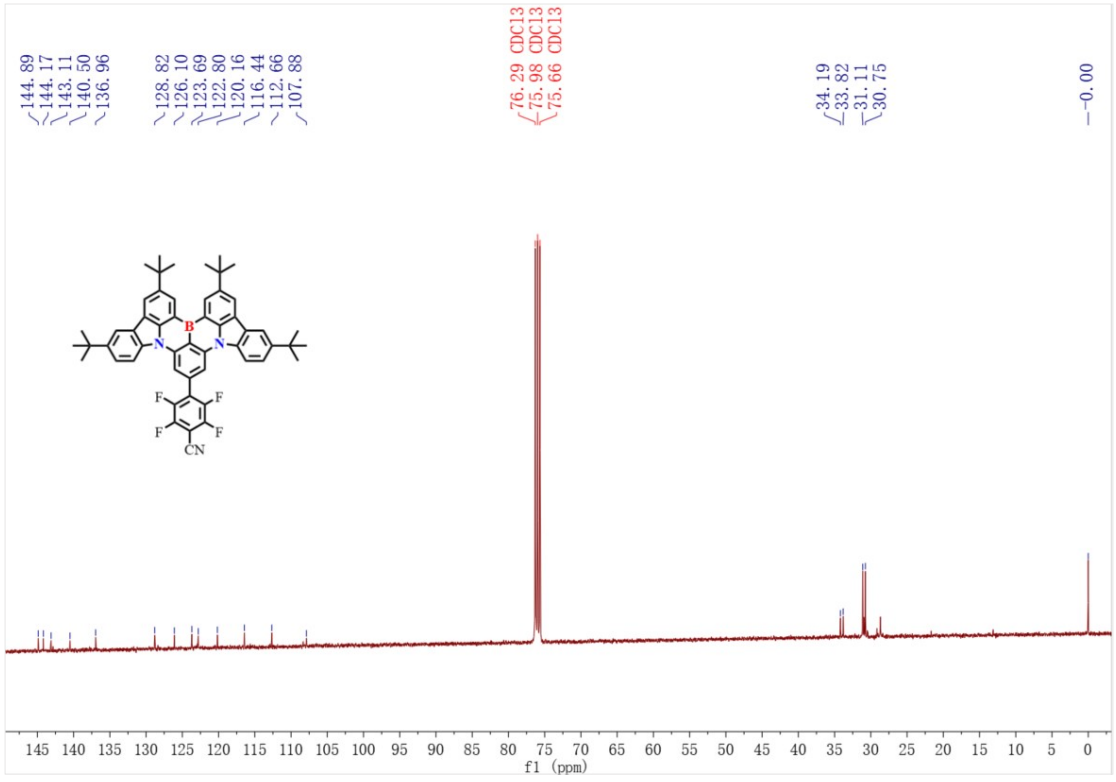

Fig. S3.^{13}C-NMR spectrum of compound 4TCzBNCN in $CDCl_3$ at room temperature.

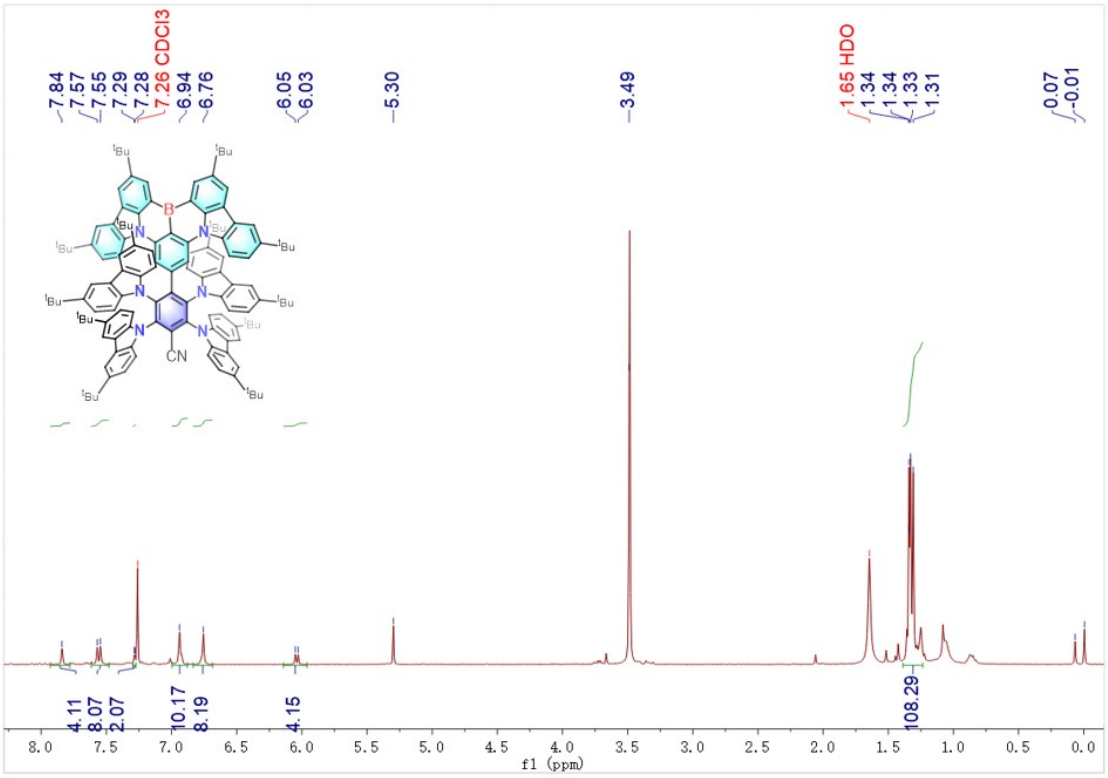

Fig. S4. ^{1}H-NMR spectrum of compound 4TCzBNCN in $CDCl_3$ at room temperature.

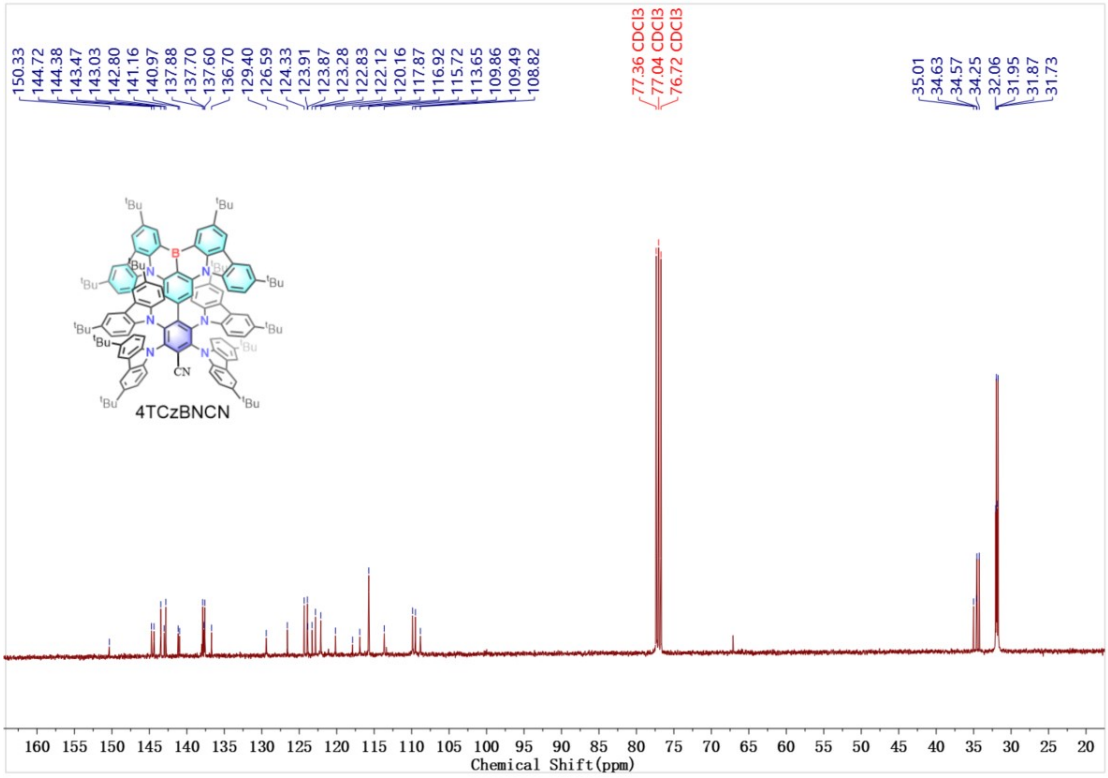

Fig. S5. ^{13}C-NMR spectrum of compound 4TCzBNCN in $CDCl_3$ at room temperature.

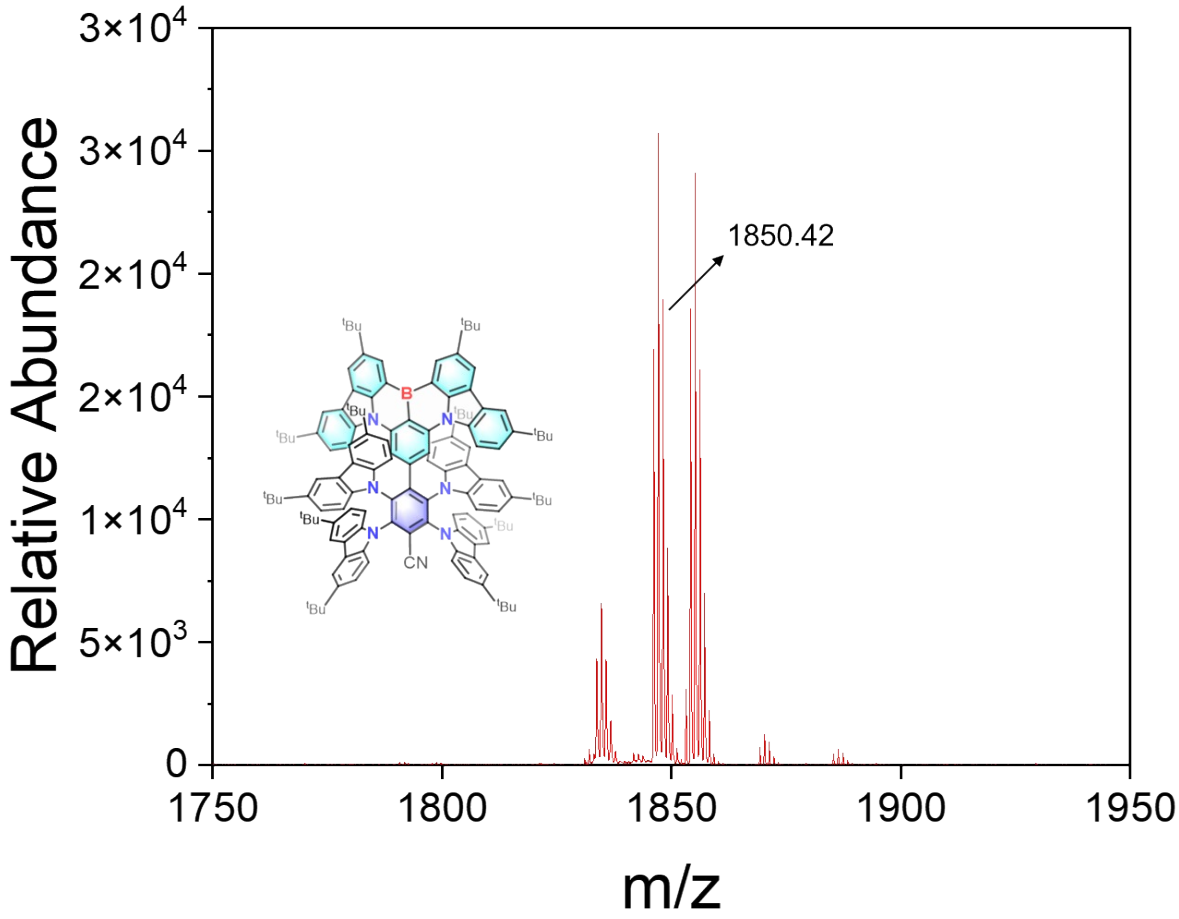

Fig. S6. HR-MS spectrum of 4TCzBNCN.

3. Figures and Tables

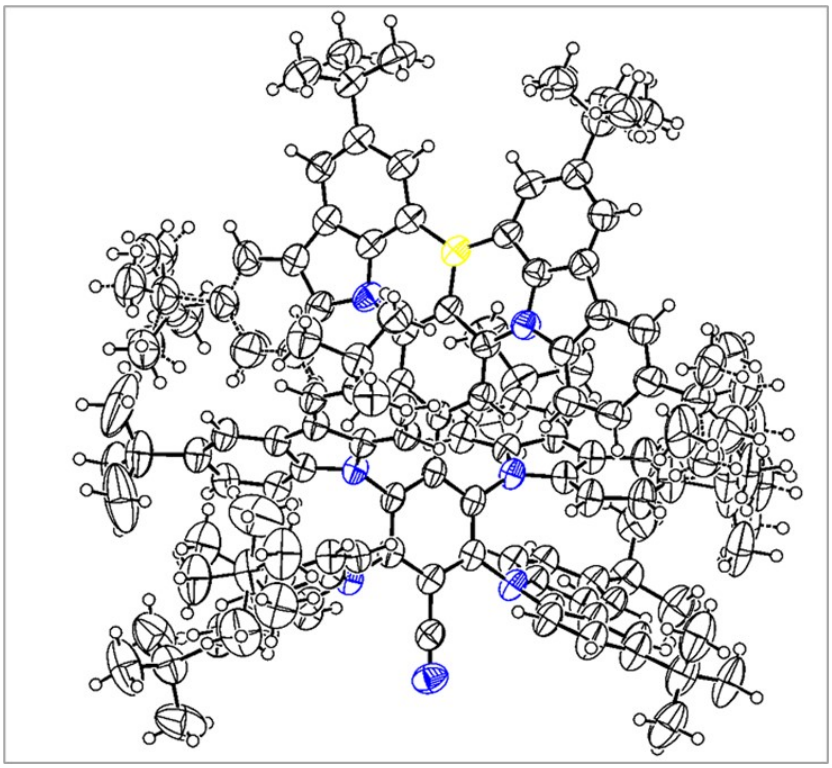

Fig. S7. Ellipsoid plot of 4TCzBNCN obtained by single crystal diffraction.

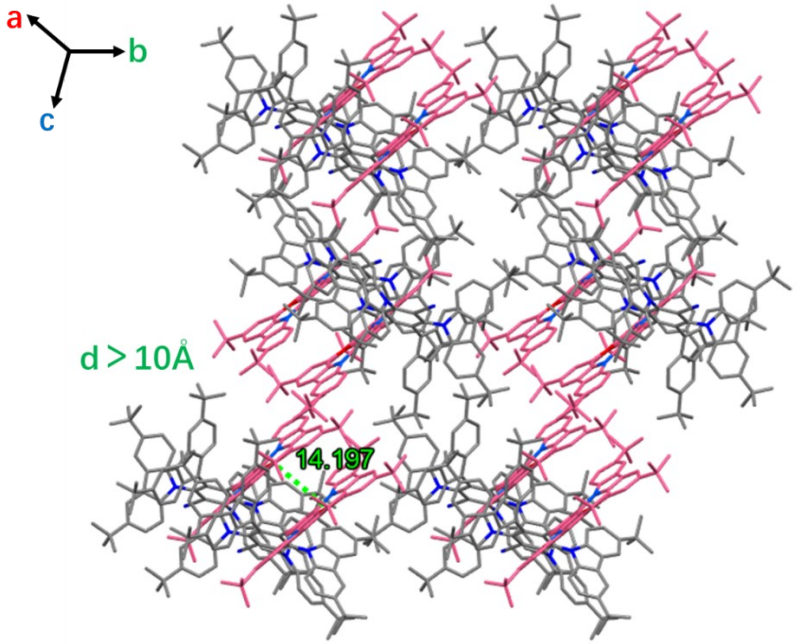

Fig. S8. Single crystal packing mode of 4TCzBNCN.

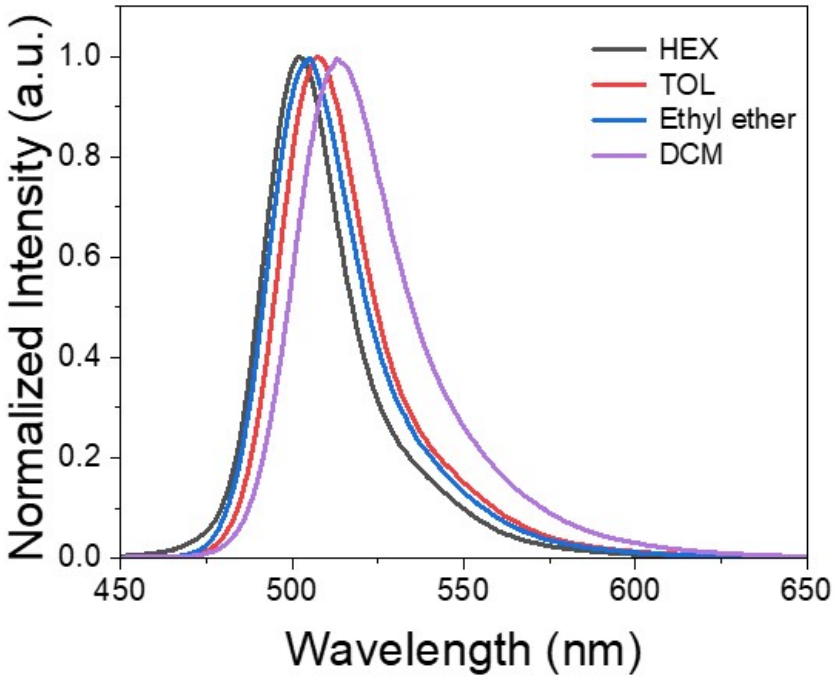

Fig. S9. Fluorescence spectra (300 K) of 4TCzBNCN measured in different solvents (1 × 10^{-5} mol L^{-1}).

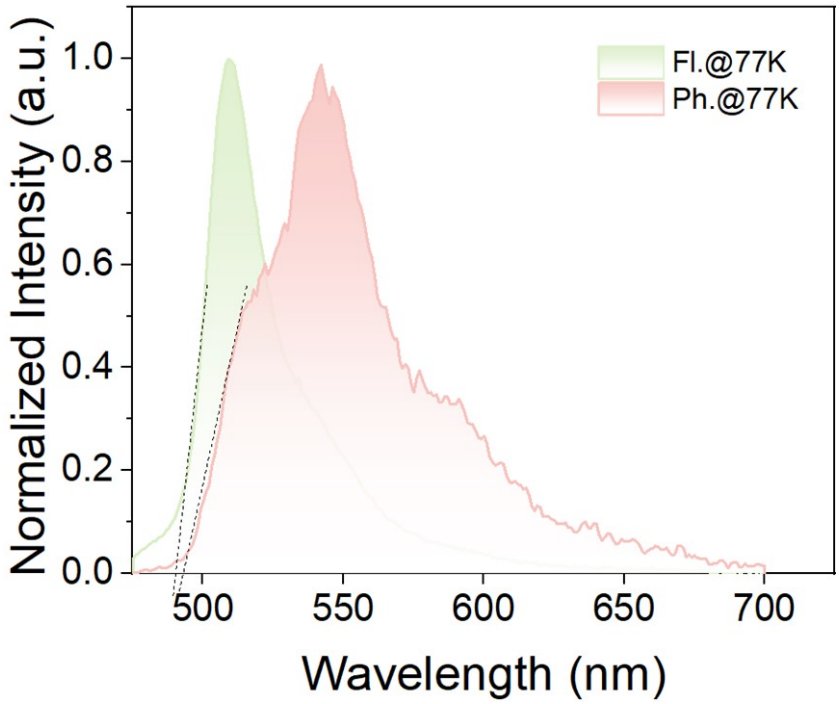

Fig. S10. Fluorescence and phosphorescence spectra (77 K) of 4TCzBNCN in toluene solution (1 × 10^{-5} mol L^{-1}).

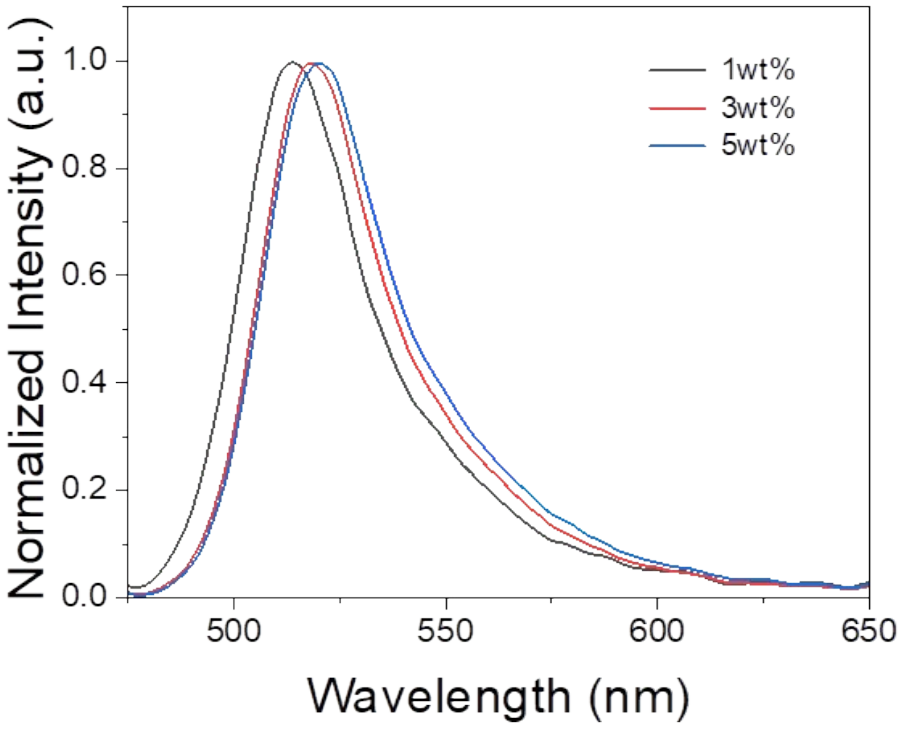

Fig. S11. Concentration-dependent PL of 4TCzBNCN in PhCzBCz doped films

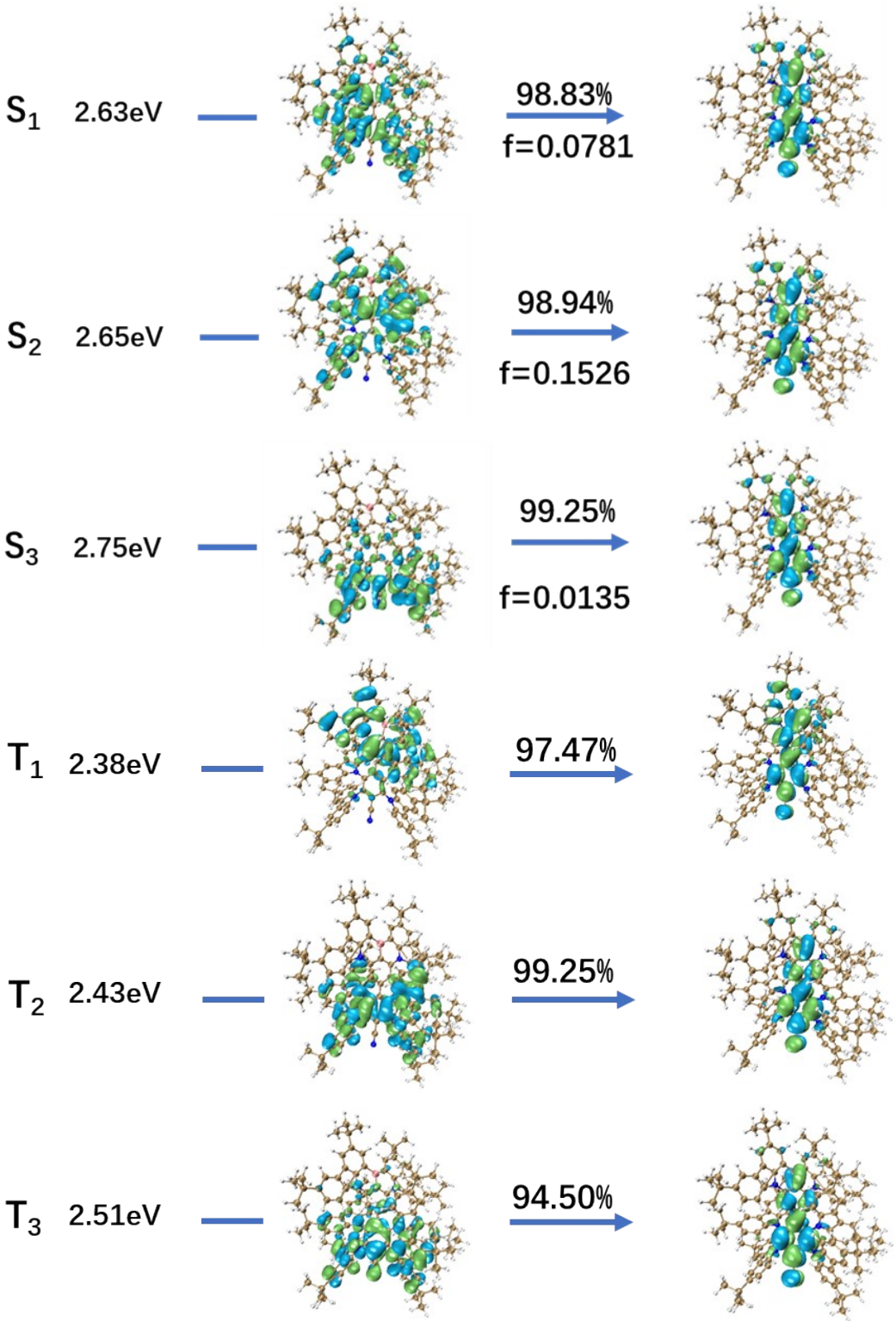

Fig. S12. The NTO diagram of 4TCzBNCN.

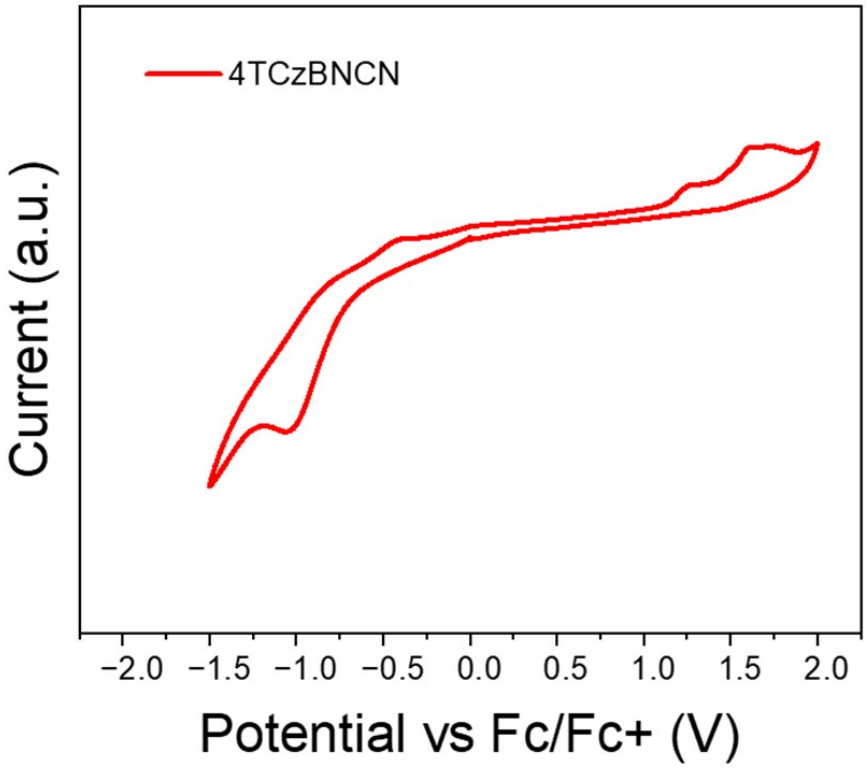

Fig. S13. Cyclic voltammetry curves for 4TCzBNCN.

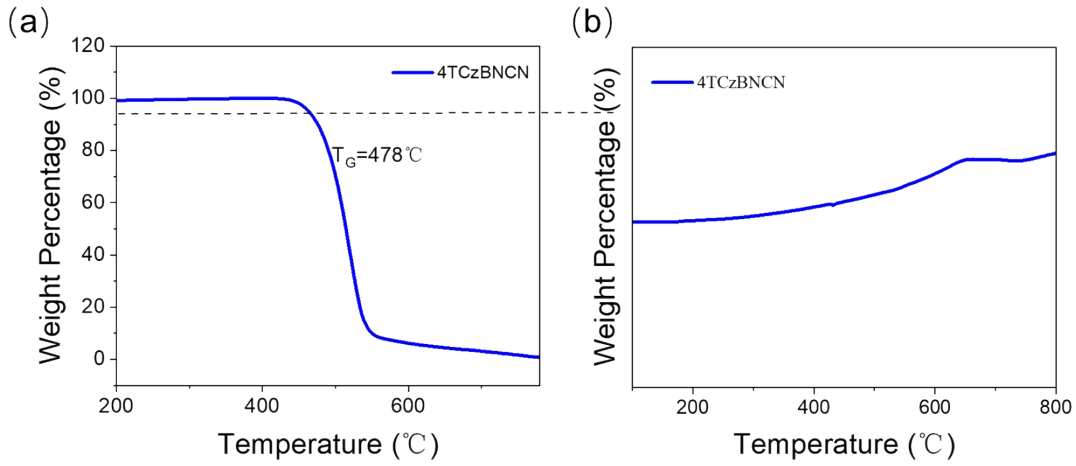

Fig. S14. (a)TGA curves of 4TCzBNCN at a heating rate of 10℃min^{-1} under N_2; (b) DSC profiles of 4TCzBNCN in the aggregated states.

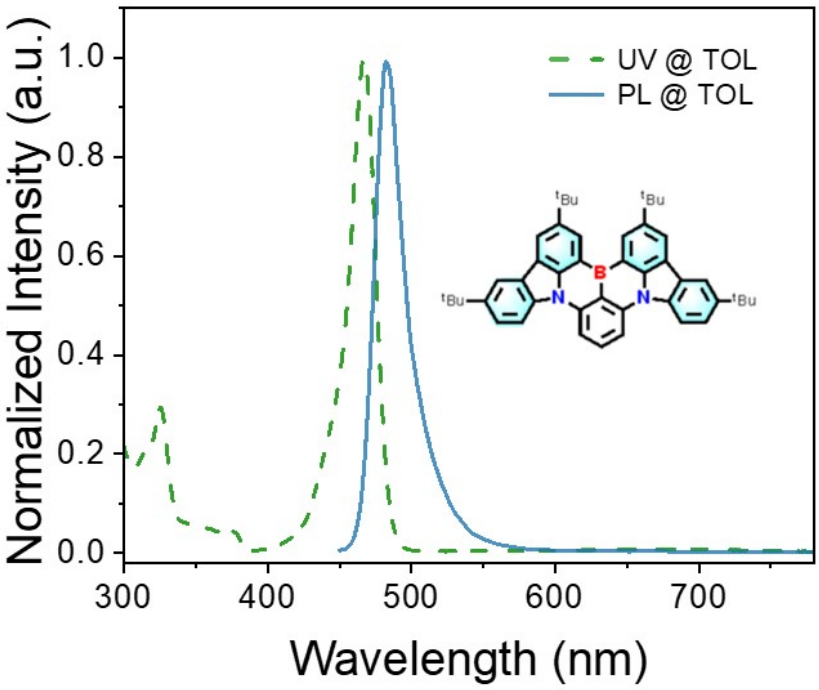

Fig. S15. UV-vis absorption and fluorescence (FL) spectra (300 K) of BCz-BN in toluene solution (1×10^{-5} mol L^{-1}).

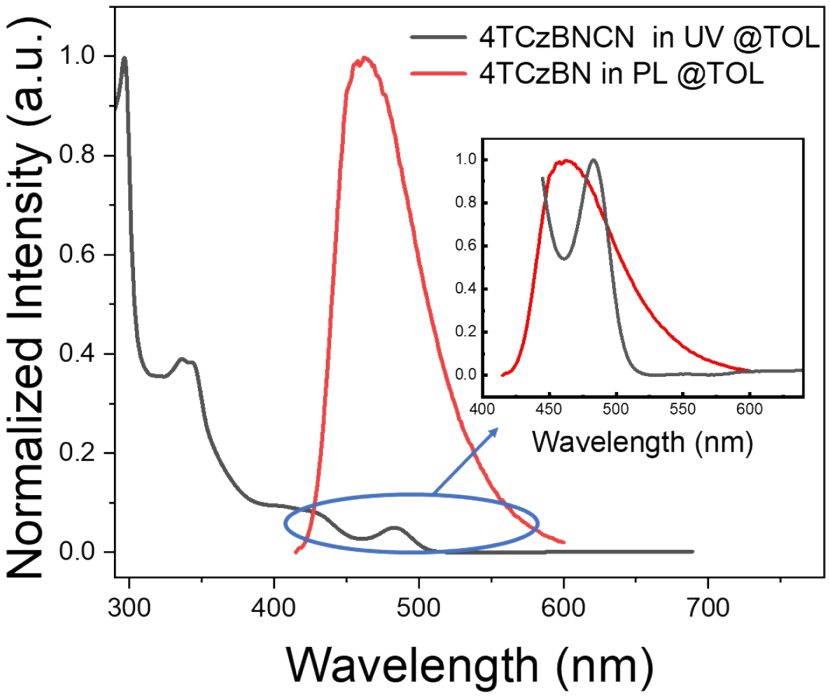

Fig. S16. UV-vis absorption of 4TBCzBNCN and fluorescence (FL) spectra (300 K) of 4TCzBN in toluene solution (1×10^{-5} mol L^{-1}).

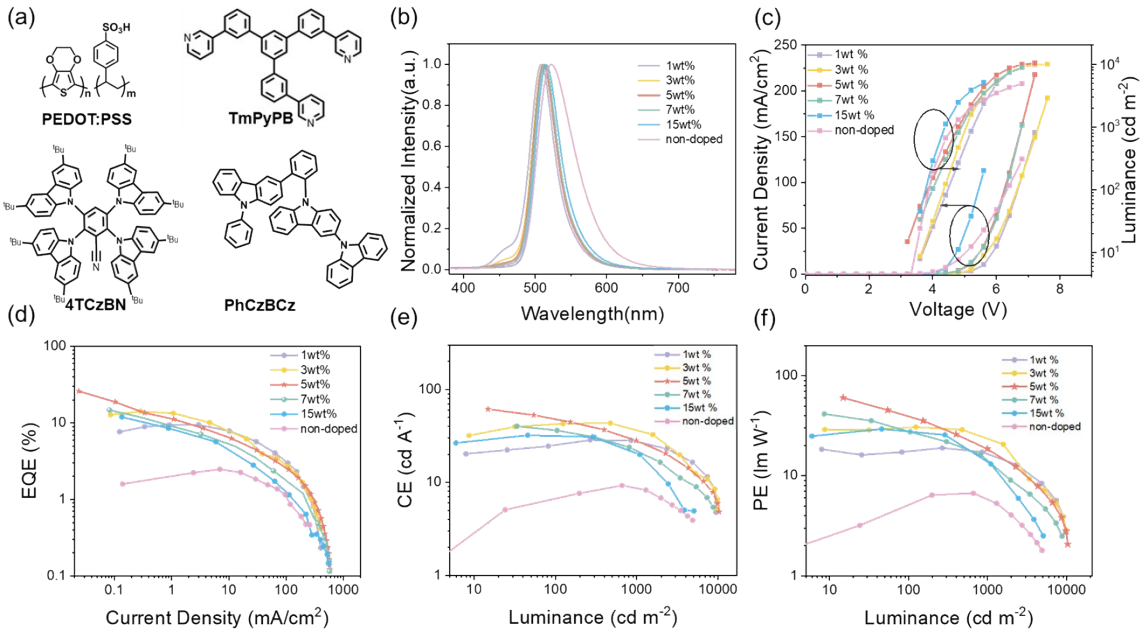

Fig. S17. a) Molecular structures employed in the devices. b) EL spectra for six solution-processed devices. c) J-V-L curves for six solution-processed devices. d) EQE as a function of Current Density for six solution-processed devices. e) CE as a function of luminance for six solution-processed devices. f) PE as a function of luminance for six solution-processed devices

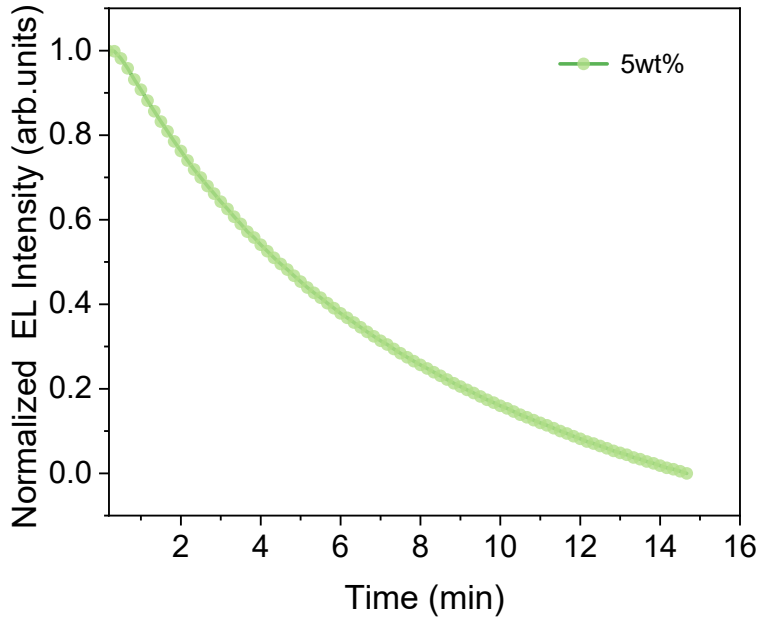

Figure S18: Lifetime decay of a solution-processed 4TCzBNCN OLED under continuous operation.

It is worth noting that these results were obtained under non-ideal conditions. Due to equipment limitations, the unencapsulated device was transported in an argon-filled container for a full day before testing. Despite this, it remained operational at 1000 cd m^{-2}, and we expect its stability would be significantly improved with proper encapsulation and timely testing.

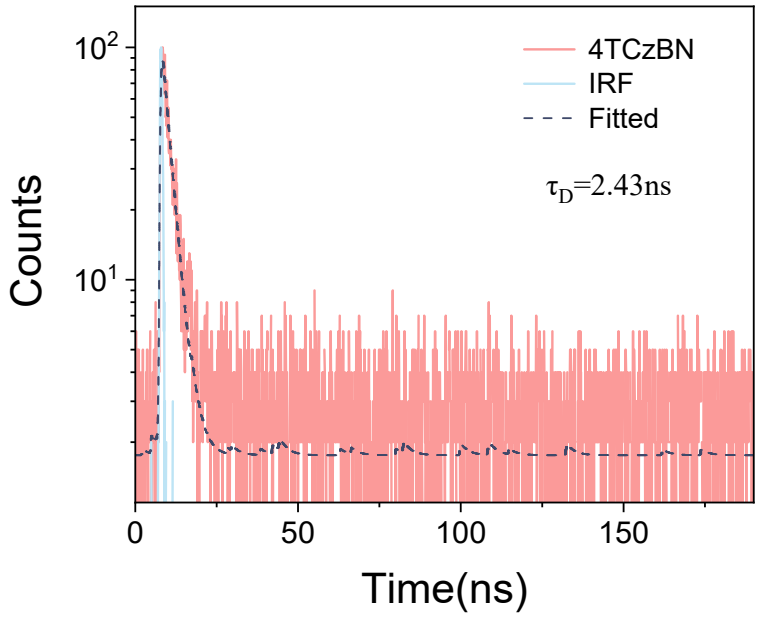

Figure S19: Transient PL decay profile of 4TCzBN neat flim at 300 K (λ_{ex} = 400 nm)

Table S1. Crystal data and structure of 4TCzBNCN.

CCDC	2481073
Empirical formula	$C_{133}H_{144}BN_7$
Formula weight	1851.35
Temperature/K	150
Crystal system	triclinic
Space group	P 1 21/n 1
a/Å	14.1966(6)
b/Å	18.2589(8)
c/Å	27.0023(12)
α/°	103.529(2)
β/°	98.747(3)
γ/°	105.155(2)
Volume/Å^3	6396.7(5)
Z	2
ρ_{calc} g/cm^3	0.961
μ/mm^{-1}	0.416
F(000)	1992.0
Crystal size/mm^3	0.15 × 0.08 × 0.05
2Θ range for data collection/°	1.994 to 26.395
Index ranges	$-19 \le h \le 19$, $-14 \le k \le 16$, $-38 \le l \le 34$
Reflections collected	48503
Independent reflections	13091 [$R_{(int)}$ = 0.0899]
Data/restraints/parameters	13091/0/679
Goodness-of-fit on F^2	1.037
Final R indexes [I>=2σ (I)]	R_1 = 0.0676, wR_2 = 0.1588
Final R indexes [all data]	R_1 = 0.1238, wR_2 = 0.1870
Largest diff. peak/hole / e Å^{-3}	0.207/-0.251

The calculation formulas for the rate constants of fluorescent (k_F), internal conversion (k_{IC}), intersystem crossing (k_{ISC}), TADF (k_{TADF}) and reverse intersystem crossing (k_{RISC}) are expressed as following list. Assume the non-radiative decay rate of the triplet state is zero. ($k_{T,nr} = 0$).

$$\Phi = \Phi_{DF} + \Phi_{PF} \quad (1)$$

$$K_r = \Phi_{PF}/\tau_{PF} \quad (2)$$

$$K_{RISC} = K_F K_{DF} \Phi_{DF}/k_{ISC}\Phi_F \quad (3)$$

Table S2. Excited state energies, energy gaps and corresponding spin-orbit coupling matrix elements ($<S_1|\hat{H}_{SOC}|T_1>$ and $<S_1|\hat{H}_{SOC}|T_2>$) for 4TCzBNCN and BCz-BN at the B3LYP/6-31G(d) level.

Compound	S_1 (eV)	T_1 (eV)	$\Delta E_{S1\text{-}T1}$ (eV)	HOMO/LUMO /E_g [eV]	$<S_1\|\hat{H}_{SOC}\|T_1>$ (cm^{-1})	$<S_1\|\hat{H}_{SOC}\|T_2>$ (cm^{-1})
4TCzBNCN	2.64	2.51	0.13	-5.17/-2.04/3.13	0.370	0.190
BCz-BN	2.86	2.46	0.4	-5.07/-1.72/3.35	0.028	0.014

Table S3. OLEDs' performance based on 4TCzBNCN.

Devices	V_{on} [a] [V]	L_{max} [b] [cd m^{-2}]	CE_{max} [c] [cd A^{-1}]	PE_{max} [c] [lm W^{-1}]	EQE[d] [%]	Peak [e] [nm]	FWHM [e] [nm]	CIE [e] [x, y]
1wt%	3.6	9687	29.1	19.0	9.6	508	40	(0.15,0.55)
3wt%	3.6	9912	44.2	30.7	13.6	512	40	(0.17,0.63)
5wt%	3.2	10320	61.7	60.4	26.8	512	38	(0.16,0.63)
7wt%	3.6	8751	40.8	35.5	15.1	514	39	(0.17,0.65)
15wt%	3.6	5061	33.7	29.3	11.4	516	41	(0.19,0.66)
non-doped	3.2	4882	3.89	1.80	1.57	523	60.2	(0.27,0.64)

[a] Turn-on voltage. [b] Maximum luminance. [c] Maximum current efficiency and power efficiency. [d] Maximum EQE. [e] EL peak, FWHM, and CIE color coordinates.

Table S4. Calculated spin–orbit coupling matrix elements (SOCMEs) and energy gaps between S_1 and T_n states for 4TCzBNCN

State	Energy (eV)	$\Delta E_{(Tn-S1)}$ (eV)	SOCME (cm^{-1})
S_1	2.64	/	/
T_1	2.51	0.13	0.370
T_2	2.43	0.19	0.190
T_3	2.51	0.13	0.312
T_4	2.79	-0.15	0.457

Note： Energies were obtained from TD-DFT calculations at the B3LYP/6-31G(d) level. Spin–orbit coupling matrix elements (SOCMEs) were calculated at the optimized S_1 geometry. $\Delta E_{(T_n-S_1)}$ denotes the energy difference between the nth triplet excited state and the lowest singlet excited state (S_1). Positive ΔE values indicate that the corresponding

triplet state lies below S_1.

Evaluation of energy transfer from host to guest

The rate of energy transfer k_{ET} from a host to a guest and the efficiency of Förster energy transfer Φ_{ET} can be calculated as following equations:

$$k_{ET} = \frac{1}{\tau_D}\frac{R_0}{(R_{hg})^6} \quad (4)$$

$$\Phi_{ET} = \frac{k_{ET}}{k_{ET} + \frac{1}{\tau_h}} = \frac{1}{1 + \left(\frac{R}{R_0}\right)^6} \quad (5)$$

where τ_h is the decay time of the host in the absence of the guest, R_0 is the Förster radius and R_{hg} is the host-to-guest distance. Among them, the Förster radius (R_0), critical distance for the concentration quenching could be estimated by using the following equation:

$$R_0^6 = \frac{9000(\ln 10)k^2\Phi_{PL}}{128\pi^5 N_A n^4}\int_0^\infty F_h(\lambda)\varepsilon_g(\lambda)\lambda^4 d\lambda \quad (6)$$

where k^2 is orientation factor (k^2 is typically assumed to be 2/3 for the random orientation system), Φ_{PL} is the quantum yield of the host in the absence of the guest, N_A is Avogadro's number, n is the refractive index of the medium, $\int_0^\infty F_h(\lambda)\varepsilon_g(\lambda)\lambda^4 d\lambda$ is the spectral overlap integral between host PL [$F_h(\lambda)$] and guest absorption [$\varepsilon_g(\lambda)$] in which $F_h(\lambda)$ is the host's fluorescence normalized by area, $\varepsilon_g(\lambda)$ is the molar decadic extinction coefficient of the guest, and λ is the wavelength. And the distance between the host and guest (R_{hg}) can be calculated by using:

$$R_{hg} = \left(N_g \times \frac{4\pi}{3}\right)^{-\frac{1}{3}} \quad (7)$$

where N_g is the quantity of guest molecules in a unit volume, which is in direct

proportion to the guest doping concentration. According to Samuel's report, the density of chromophores can be described as

$$N_g = \beta \times \rho \times {}^{N_A}/_{M_C} \qquad (8)$$

where β is the fraction of guests present in the film, ρ is the density of the film (assumed to be 1 g cm^{-3}), N_A is Avogadro's number and M_C is the molecular weight of the guest.

Based on the Förster resonance energy transfer (FRET) model, the energy transfer from 4TCzBN to 4TCzBNCN was quantitatively analyzed using the prompt fluorescence lifetime of pristine 4TCzBN (2.43 ns, refer to Figure S19) as the donor lifetime. The relevant data are summarized in Table S5.

Table S5. Summary of energy transfer parameters of the PhCzBCz: 4TCzBN: 4TCzBNCN doping system.

Concentration[a)]	R_0 [nm]	R_{hg} [nm]	Φ_{ET} [%]	k_{ET} [×10^9 S^{-1}]
5 wt%	3.94	2.45	94.59	7.19

[a)]Abbreviations: R_0 = Förster energy transfer radius; R_{hg} = distance between the host (h) and guest (g); k_{ET} = the Förster energy transfer rate; Φ_{ET} = the Förster energy transfer efficiency.